THE ASTROPHYSICAL JOURNAL, 442:597–609, 1995 April 1

THE ORIGIN OF THE SOFT X-RAY EXCESS IN THE SEYFERT 2 GALAXY NGC 2110

K. A. WEAVER,[1,2] R. F. MUSHOTZKY, AND P. J. SERLEMITSOS
NASA/Goddard Space Flight Center, Code 666, Greenbelt, MD 20771
A. S. WILSON[2]
Space Telescope Science Institute, 3700 San Martin Drive, Baltimore, MD 21218
M. ELVIS
Harvard-Smithsonian Center for Astrophysics, Cambridge, MA 02138
AND
U. BRIEL
Max-Planck-Institut für Extraterrestrische Physik, D-85748 Garching, Germany
Received 1994 July 11; accepted 1994 October 10

ABSTRACT

We present and discuss an X-ray image and a medium-resolution X-ray spectrum of the Seyfert 2 galaxy NGC 2110 obtained with the high-resolution imager (HRI) on *ROSAT* (0.1–2.4 keV) and Goddard's Broad Band X-Ray Telescope (BBXRT; 0.3–11 keV), respectively. Spatially resolved soft X-ray emission, which peaks 4″ to the north of the nucleus and near the position of the highest excitation optical emission line gas, is seen in the HRI observation. The extent has a flux of $\sim 3 \times 10^{-13}$ ergs cm^{-2} s^{-1} and accounts for 11% ± 3% of the total 0.1–2.4 keV flux. To model the BBXRT spectrum, a soft excess component is required which has a flux of $\sim 3.5 \times 10^{-13}$ ergs cm^{-2} s^{-1} and accounts for ∼14% ± 6% of the total 0.1–2.4 keV flux. In addition, BBXRT confirms the presence of an ∼175 eV equivalent width Fe Kα fluorescence line in NGC 2110.

Because of the good agreement between their fluxes, we propose that the soft excess arises from the spatially resolved X-ray emission. This is contrary to previous suggestions that the spectral soft excess in NGC 2110 is due to leakage of the X-ray continuum through a patchy absorber. The temperature of the gas responsible for the soft excess is too high to be accounted for by local shock heating. In order to explain the soft excess and extent as either scattered continuum X-rays or fluorescence from gas photoionized by the nuclear source, the hard X-rays must be emitted anisotropically. However, the soft excess and extent can be well modeled as thermal emission from a hot, outflowing wind, which may also be responsible for confining at least some portion of the optical narrow line–emitting clouds.

Subject headings: galaxies: individual (NGC 2110) — galaxies: ISM — galaxies: nuclei — galaxies: Seyfert — radiation mechanisms: nonthermal — X-rays: galaxies

1. INTRODUCTION

The S0 galaxy NGC 2110 ($D = 47$ Mpc assuming $H_0 = 50$ km s^{-1} Mpc^{-1} and a recession velocity of $v = 2342$ km s^{-1}; de Vaucouleurs et al. 1991) is a low-ionization active galaxy (Shuder 1980) with an optical nuclear spectrum similar to that of Seyfert 2 galaxies (Bradt et al. 1978; McClintock et al. 1979). It is perhaps best described as a "transition" object with properties intermediate between LINERs and Seyfert 2 galaxies. A weak, broad component to Hα has also been claimed (Shuder 1980).

Imaging and spectroscopic observations show a high-excitation nebulosity that extends over 20″ (4.6 kpc) and is photoionized by a nonstellar continuum (Wilson, Baldwin, & Ulvestad 1985; Pogge 1989). The [O III] λ5007 distribution is elongated from north to south and extends asymmetrically toward the north. "Excitation maps" of the flux ratio [O III] λ5007/(Hα + [N II] λλ6548, 6584) (Pogge 1989; Haniff, Ward, & Wilson 1991) reveal that the highest excitation gas is located to the north, about 4″–5″ from the nucleus. Spectroscopic observations (Wilson et al. 1985, Fig. 7) also show that the gaseous excitation is much higher to the north of the nucleus than either at the nucleus or to the south. In addition, Wilson et al. (1985) found that if the spectrum of the ionizing radiation (as determined from the Hβ luminosity) is extrapolated to optical wavelengths, it predicts a flux more than three orders of magnitude greater than the observed upper limit to the nonstellar continuum at $\lambda = 3900$ Å. This result implies that either our view of the continuum source is obscured, as is also evidenced by the large X-ray–absorbing column (see below), or the ionizing photons escape anisotropically, or both. NGC 2110 also contains a small (∼5″ = 1.1 kpc) S-shaped jetlike continuum radio source (Ulvestad & Wilson 1983). The initial jet position angle (p.a. ∼0°) is roughly aligned with both the [O III] λ5007 and the Hα + [N II] emission-line distributions.

The spectral and temporal X-ray properties of NGC 2110 strongly resemble those of moderate-luminosity Seyfert 1 galaxies. NGC 2110 is a luminous, hard X-ray emitter ($L_X \sim 10^{43}$ ergs s^{-1}; Reichert et al. 1985, Tennant 1983), and has a fairly strong Fe Kα emission line (equivalent width [EW] ∼160 eV; Nandra & Pounds 1994). *HEAO* 1 A-2 data show the 2–40 keV flux from NGC 2110 to be variable on a 6 month timescale (Mushotzky 1982), implying that the hard X-rays must originate within ∼0.2 pc of the central source. The X-ray spectrum of NGC 2110 shows emission below ∼1 keV in excess of that predicted from a simple extrapolation to lower energies of the 2–10 keV power-law continuum, absorbed by a uniform

[1] Present address: Department of Astronomy and Astrophysics, 525 Davey Lab, Pennsylvania State University, University Park, PA 16802.
[2] Also Astronomy Department, University of Maryland, College Park, MD 20742.

$\sim 10^{22}$ cm^{-2} column of cold gas. This "soft excess" has been modeled as "leakage" of the continuum between clouds partially covering the nuclear source (Reichert et al. 1985; Turner & Pounds 1989). An alternative explanation, suggested by Turner & Pounds (1989), is that the soft excess comprises a physically distinct, unabsorbed component. NGC 2110 was observed with the *Einstein Observatory* HRI, but was marginally detected with a signal-to-noise ratio of only 2.4 (Garcia et al. 1990). No information about the spatial structure of the galaxy can be obtained from this observation.

In this paper we present new spatial and spectral X-ray data for NGC 2110 obtained with the *ROSAT* (high-resolution imager (HRI) and the Broad Band X-Ray Telescope (BBXRT). We discuss the analysis of the HRI data in § 2 and investigate the correlation of the X-ray emission with the radio continuum and optical emission line distributions. In § 3.1 we give a summary of the BBXRT detector characteristics, background subtraction, and data analysis procedures; in § 3.2 we present our spectral results. A discussion of the combined spectral and spatial results in the context of possible origins for the soft X-ray excess and spatial extent is contained in § 4. Our conclusions are summarized in § 5.

2. THE *ROSAT* HRI IMAGE: ANALYSIS AND RESULTS

NGC 2110 was observed on-axis with the *ROSAT* HRI for a total integration time of 31,390 s on 1991 October 3. The HRI image of the NGC 2110 field with the BBXRT pixels superposed for later reference is shown in Figure 1. The X-ray source associated with NGC 2110 is labeled *a*, and there are two X-ray sources that are located within 6′ of NGC 2110, labeled *b* and *c*. Source *b* is a bright point source located 340″ to the west and 46″ to the south of NGC 2110 [(2000) R.A. = $+5^h51^m48^s.7$, decl. = $-7°28'13''$] with a count rate of $(8.0 \pm 1.2) \times 10^{-3}$ counts s^{-1}. This source is most likely a star, although the identification is uncertain in the *HST* guide star catalog. Source *c* is an A star located ∼4′ to the north of NGC 2110 [(2000) R.A. = $+5^h52^m11^s.7$, decl. = $-7°23'30''$], with an HRI count rate of $(3.8 \pm 0.8) \times 10^{-3}$ counts s^{-1}. The mirror assembly plus HRI detector provide a spatial resolution of ∼4″–5″. However, point sources in the field show extents of ∼5″–6″ in the east-west direction, apparently resulting from residual errors in the aspect solution. This broadening makes comparisons with the standard point-spread function (PSF) misleading. Therefore, we used source *b*, which has a peak flux of about 90% of the peak flux of NGC 2110, as the PSF. Figure 2*a* shows the X-ray contours for NGC 2110 smoothed with a 5″ FWHM Gaussian. Figure 2*b* shows the point source on the same scale after smoothing with the same function. NGC 2110 clearly appears to be elongated in the north-south direction as compared to the image of the point source. The slight east-west elongation in the core of the PSF image is in a direction roughly perpendicular to the north-south elongation seen in the galaxy.

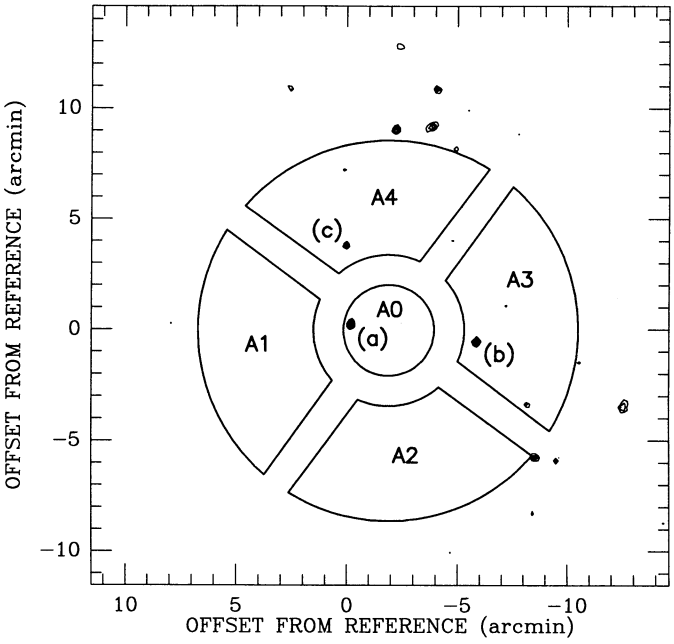

FIG. 1.—Contour map of the *ROSAT* HRI image of the NGC 2110 field with the BBXRT field of view (the A detector pixels) superposed. Contour levels are 5%, 10%, 15%, 20%, 30%, 40%, 60%, and 80% of the peak flux of NGC 2110. The sources that are discussed individually in the text are labeled according to (*a*) NGC 2110, (*b*) an X-ray point source used as the HRI PSF, and (*c*) an A star ∼5′ to the north of NGC 2110.

To assess the significance of the "extent" in NGC 2110, a cut was made through the center of NGC 2110 and the PSF in the north-south direction, and the average numbers of counts per pixel were compared in 2″ × 6″ rectangular spatial bins. A plot of the north-south cross section of the NGC 2110 image and the PSF is shown in Figure 3*a*. The off-nuclear positions where the optical ionization reaches a maximum are indicated with arrows (Haniff et al. 1991). Figure 3*b* shows the north-south cross section of the NGC 2110 image after subtraction of the scaled PSF image, along with the cross section of the PSF scaled to match the peak flux of the extent. Fitting the residuals with a scaled PSF shows that the extended emission is consistent with being a second point source located 4″ ± 1″ to the north of the nucleus [position of nucleus (2000) R.A. = $5^h52^m11^s.4$, decl. = $-7°27'26''$] with an upper limit to its size of 8″ in diameter. Although it is possible that there may be a serendipitous X-ray point source located near the position of the nucleus of the galaxy, the probability of such a chance coincidence being responsible for the spatial extent is very small. Assuming an energy index of $\alpha = 1.0$ and the Galactic column of $N_H(\mathrm{Gal}) = 1.86 \times 10^{21}$ cm^{-2} (Elvis, Lockman, & Wilkes 1989), we find a flux of 2×10^{-13} ergs cm^{-2} s^{-1} for the extended component. At this flux level, we expect $\sim 7 \times 10^{-3}$ serendipitous sources within 10′ of NGC 2110 (Hasinger, Schmidt, & Trümper 1991).

To produce an image of the extended emission in the galaxy, the flux of the PSF was scaled by a few percent and the PSF was then aligned with the peak of the NGC 2110 image and subtracted from it. This procedure was repeated several times in order to investigate the sensitivity of the subtracted image to the chosen scaling factor and alignment. It was found that the gross features of the subtracted image are quite insensitive to the exact choice of these parameters. A gray-scale map of the HRI image that results from subtracting the PSF is shown in Figure 4, with the [O III] λ5007/(Hα + [N II]) "excitation" map and 6 cm radio contours superposed. We have assumed that the nuclear X-ray source coincides with the optical nucleus (cf. Fig. 2*a*), represented by the plus sign in the center of the radio contours. As noted above, the emission region is centered 4″ (∼920 pc) to the north of the nucleus and has a maximum diameter of ∼8″ or ∼1.84 kpc (the reality of any X-ray emission beyond 4″ from the center of the black area is uncertain). The outer edge of the black area of the gray-scale

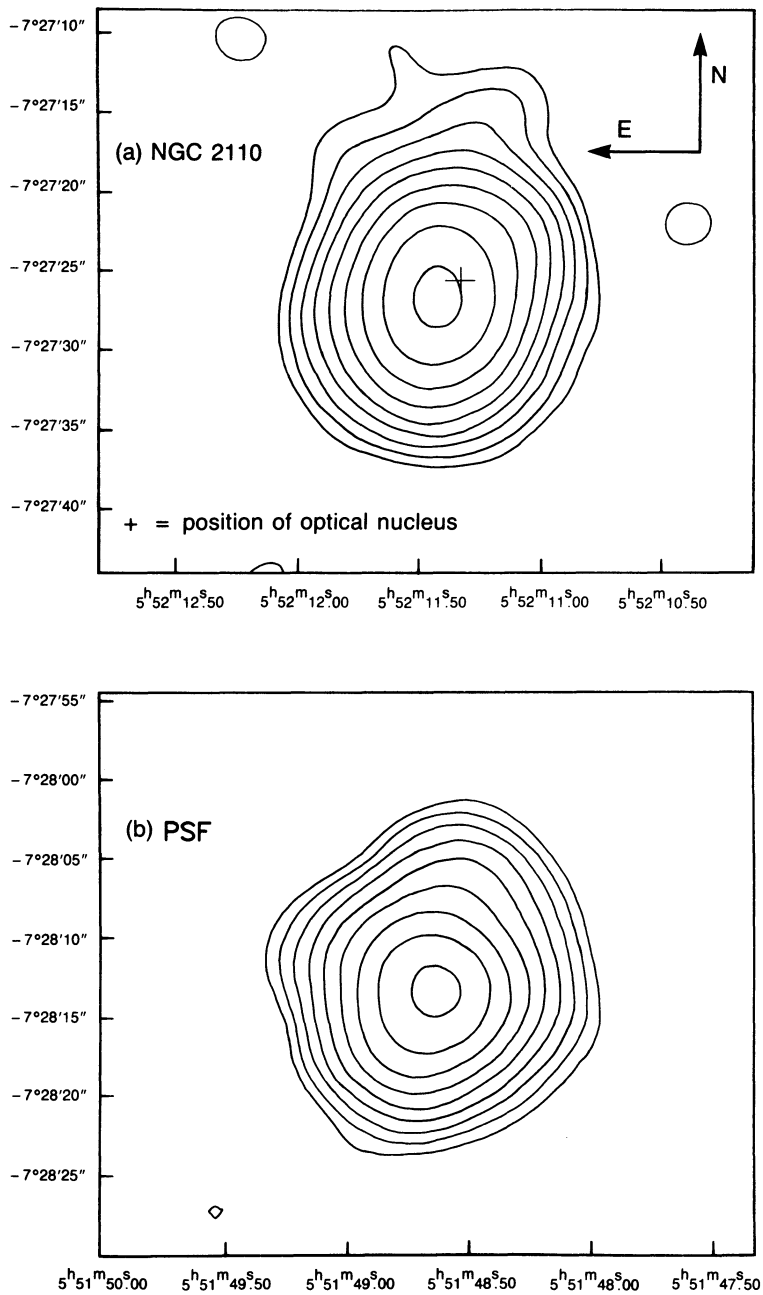

FIG. 2.—HRI X-ray contours for (*a*) NGC 2110 and (*b*) the nearby point source that was used as the PSF. Coordinates are for epoch J2000.0. The data have been smoothed with a 5″ FWHM Gaussian. Contours shown are 3%, 5%, 7%, 10%, 16%, 25%, 40%, 60%, and 90% of the peak brightness. The position of the optical nucleus (from Clements 1983) is shown as the plus sign in (*a*). The ~2″ displacement from the X-ray peak is consistent with the known errors in the X-ray astrometry.

map corresponds to ~2% of the peak brightness of the X-ray source before the subtraction of the PSF (6.0 counts pixel^{-1}; 1 pixel = 0.″5 × 0.″5). It is notable that the extended X-rays are located at the position of the highest excitation optical emission line gas. This proximity suggests a close association between the extended soft X-rays and the optical line emission.

There are about 38 photons in the extended emission, which gives a count rate of $(1.2 \pm 0.2) \times 10^{-3}$ counts s^{-1} after background subtraction, and which comprises 11% ± 3% of the total 0.1–2.4 keV HRI flux from NGC 2110. The conversion of HRI count rate to flux is strongly dependent on the assumed spectral shape of the extended emission and the line-of-sight absorption. In modeling the BBXRT spectrum (§ 3.2), the observed soft excess is assumed to be absorbed by only the Galactic column of 1.86×10^{21} cm^{-2}. However, the data actually allow a column along the line of sight to the soft component of up to 8×10^{21} cm^{-2}. Using this range in column density and assuming the best-fit thermal bremsstrahlung ($T = 5 \times 10^6$ K) or Raymond-Smith ($T = 1 \times 10^7$ K) modeling of the BBXRT soft excess (§ 3.2), we find an extended flux in the HRI of $F_{ext} = 3.5^{+6.5}_{-1.0} \times 10^{-13}$ ergs cm^{-2} s^{-1} or $F_{ext} = 2.3^{+3.7}_{-1.4} \times 10^{-13}$ ergs cm^{-2} s^{-1}, respectively, corresponding to a range of luminosities, L_{ext}, between 2.3×10^{40} and 2.6×10^{41} ergs s^{-1}.

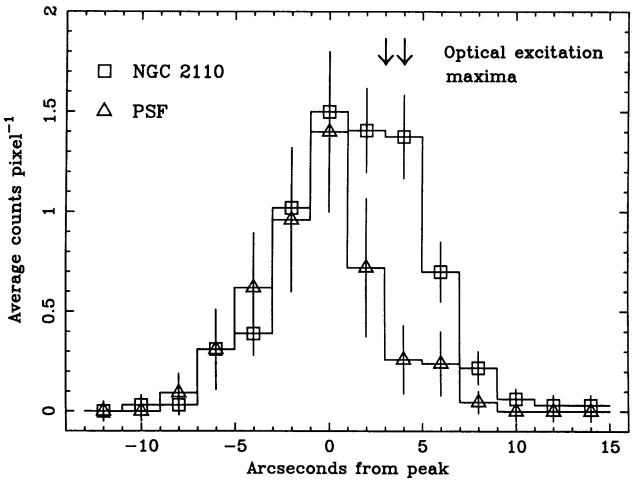

FIG. 3a

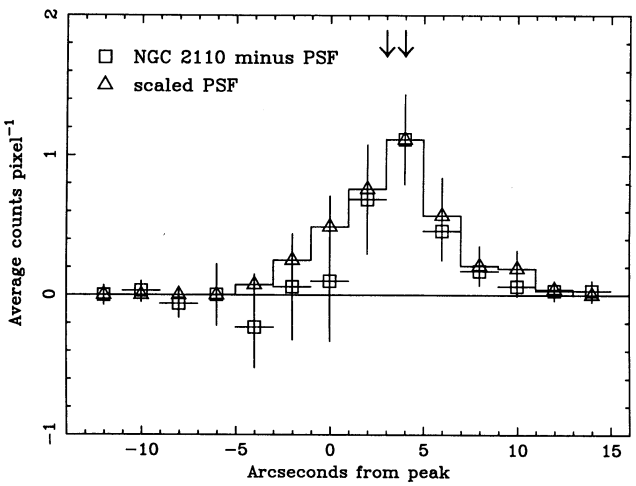

FIG. 3b

FIG. 3.—North-south cross section profile given in average number of counts per pixel for (*a*) NGC 2110 and the chosen PSF and (*b*) NGC 2110 with the PSF subtracted compared with the PSF scaled to match the peak flux of the extent. The location of the highest excitation optical emission line gas (Haniff, Ward, & Wilson 1991) is shown with arrows.

Could the absence of soft X-rays to the south of the nucleus be due to their being behind and absorbed by gas in the galaxy disk? If there is extended emission to the south with a similar flux to that observed to the north, a gaseous column of at least 1×10^{22} cm^{-2} must be present to absorb it. This is consistent with the column density of the gas absorbing the nuclear X-ray continuum source (§ 3.2) as well as the high reddening observed near the nucleus (Mulchaey et al. 1994). However, the nuclear X-ray continuum absorber is expected to be located much closer to the nucleus than the extended emission. The column of 1×10^{22} cm^{-2} required to block the X-rays is only about twice as large as the column inferred from recent *HST* measurements of a dust lane running north-south and offset by $\sim 1''$ to the west of the galaxy nucleus (Mulchaey et al. 1994). A gaseous column sufficient to photoelectrically absorb extended X-ray emission to the south is thus not implausible. However, there does appear to be an intrinsic asymmetry in the optical line emission because the [O III]/Hβ ratio, which should be sensibly independent of extinction, is higher to the north of the nucleus than to the south (Wilson et al. 1985). This result suggests that the X-ray asymmetry may also be intrinsic and not due to absorption.

3. THE BBXRT SPECTRUM

3.1. *Instrumentation, Observations, and Analysis Techniques*

BBXRT (Serlemitsos et al. 1992) flew on the space shuttle Columbia in 1990 December. The instrument consists of two telescopes with lightweight nested foil mirrors that focus X-rays onto two solid state detectors. Each BBXRT detector (designated A or B) consists of a silicon block with a grooved surface, segmenting it into five spatial elements or "pixels" (Fig. 1). The field of view of the central pixels (labeled A0 and B0) is 3.'6, and the outer pixels (labeled A1–A4 and B1–B4) extend to 8.'6 off-axis. The central pixels provide an energy resolution of ~ 100 eV at 0.9 keV and ~ 155 eV FWHM at 6 keV. The instrument provides a total bandpass of 0.3–12.0 keV and a combined central-pixel effective area of ~ 200 cm^2 at 1 keV. The effective area for the central pixels for an on-axis point source is known to within 5%–10% between 0.7 and 10.0 keV based on observations of the Crab Nebula (Weaver et al. 1995), although uncertainties of $\sim 15\%$ remain below 0.7 keV. A complete discussion of the BBXRT instrument and calibration can be found in Serlemitsos et al. (1992) and Weaver et al. (1995).

Although NGC 2110 was observed twice during the BBXRT mission, the first observation suffered from mispointing and so gave a low count rate. We use only the data from the second observation on December 9 (~ 2500 net seconds), for which more than 70% of the counts from NGC 2110 fell in the central pixels, giving a count rate of ~ 0.43 counts s^{-1} in pixel A0. The BBXRT pixels are shown superposed on the HRI image in Figure 1. No sources are seen within the central pixels to a level of 5% of the NGC 2110 source. Within the outer pixels, X-ray sources *b* and *c* are seen (§ 2), which have $\sim 35\%$ and $\sim 80\%$ of the total flux of NGC 2110 in the HRI, respectively. The BBXRT mirrors have a PSF with a 1.'3 half-power radius and extended wings, which can allow a significant fraction of the flux from sources in the outer pixels to fall into the central pixel depending on their off-axis position (Weaver et al. 1995). Source *c* within pixel A4 is located about 4′ off-axis, and so less than 5% of the counts from it are expected to fall in A0 and B0. From examining the A4 data, there is no significant detection of this source at 1 keV, so it contributes less than 2% to the NGC 2110 spectrum in A0 and is of no consequence in our analysis. The brighter source *b* located 3.'5 off-axis to the west is detected in A3 at a level of 75% of the 0.9–1.0 keV BBXRT flux of NGC 2110. This source is soft, having a spectrum modeled equally well with a $kT = 0.36^{+0.44}_{-0.19}$ keV bremsstrahlung or a steep power-law with a photon index of $4.0^{+4.0}_{-1.5}$. For a point source observed 3.'5 off-axis, as many as 8% of the photons may fall into the central pixel (Weaver et al. 1995). Therefore, source *b* contributes $\sim 6\%$ of the total flux in A0 between 0.9 and 1 keV. Such a contribution to the NGC 2110 spectrum is negligible in our spectral analysis (§ 3.2) because of the fairly poor statistics below 1 keV in both A0 and B0. Source *b* also contributes less than 2% of the NGC 2110 flux above 1 keV and so does not complicate the analysis at higher energies. The two groups of sources lying about 12′ to the north-northwest and southwest are fortunately well outside the field of view of the central BBXRT pixel.

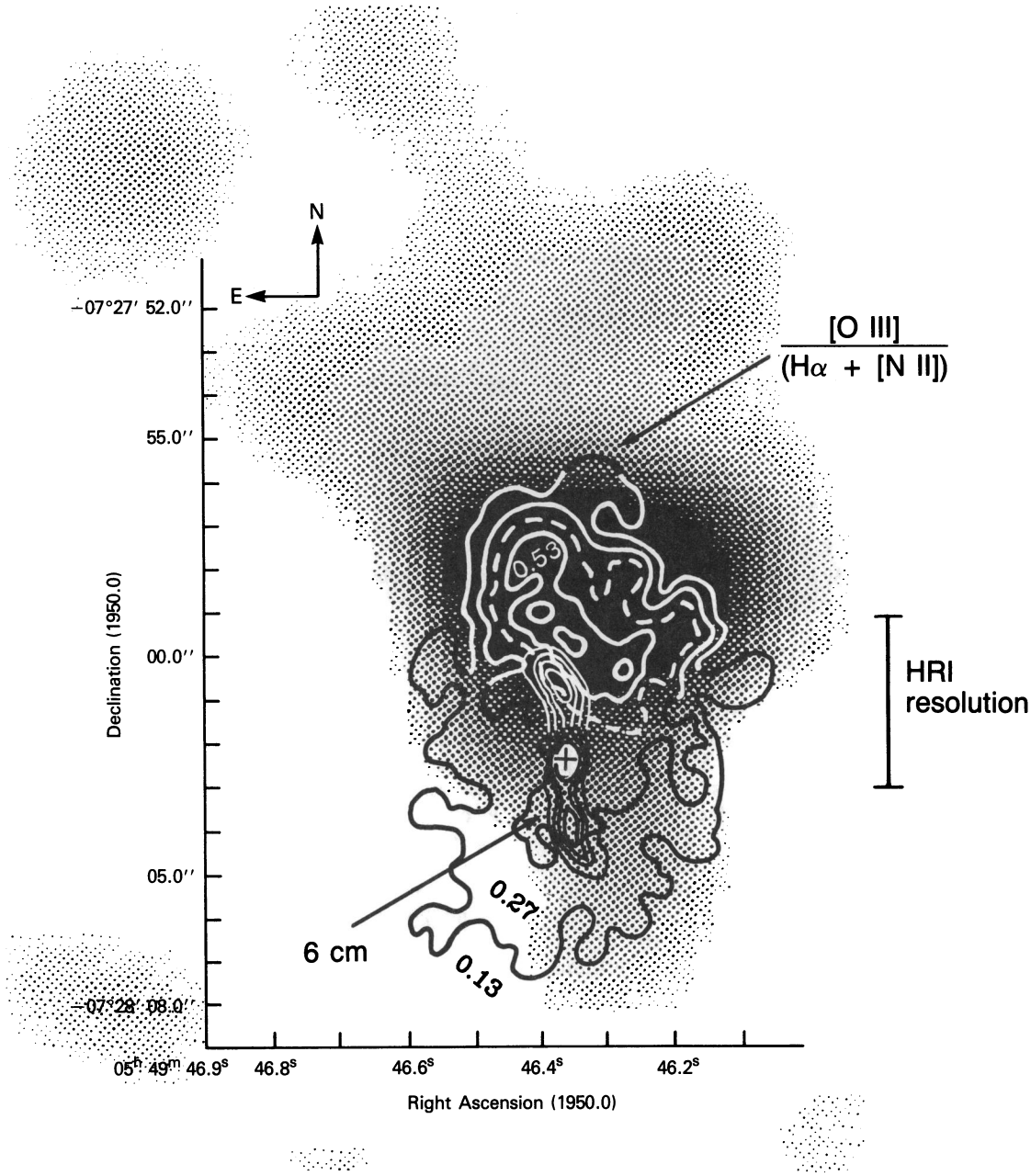

FIG. 4.—Optical and radio contours superposed on a gray-scale map of the X-ray emission that remains after subtracting the nuclear point source. Contours of the 6 cm radio map (the north-south–elongated jetlike feature) are taken from Ulvestad & Wilson (1983). The plus sign in the center of the radio contours marks the position of the optical nucleus, which is assumed to coincide with the nuclear X-ray peak. The optical contours represent the excitation ratio R = [O III] λ5007/(Hα + [N III]) from Haniff et al. (1991). The R contour levels shown are 0.13, 0.27, 0.40 (*dashed line*), and 0.53. The contours of R are uncertain near the north edge of the optical nebulosity and may not close. The excitation ratio peaks to the north of the optical nucleus, close to the extended X-ray emission.

Both the orbit-night and orbit-day BBXRT backgrounds can be estimated quite accurately. Major contributors to the BBXRT detector background are particle events, the cosmic X-ray background (CXRB), and X-ray contamination at low energies from scattered solar radiation. The contribution from the particle background is small, about 2×10^{-3} counts s^{-1} at 0.5 keV, and can be easily predicted (Jahoda et al. 1992; Weaver et al. 1995). The CXRB contribution is also small and roughly equal to the particle background at 0.5 keV. The largest contribution to the background below 1 keV is created by X-rays from the solar corona that scatter from Earth's upper atmosphere during orbit-day observations. The intensity of scattered X-rays is largest for pointings close to Earth's limb and decreases away from it (Weaver et al. 1995). The NGC 2110 observation was mostly performed during orbit night; however, the last 500 s of the observation was performed during orbit day, with the telescope pointing in a direction $\sim$45° away from Earth's limb. At that position, the major daytime contaminant is the oxygen fluorescence line at 0.525 keV (Weaver et al. 1995).

To perform background subtraction, source-free, orbit-day background (for a position $\sim$45° from Earth's limb) and orbit-

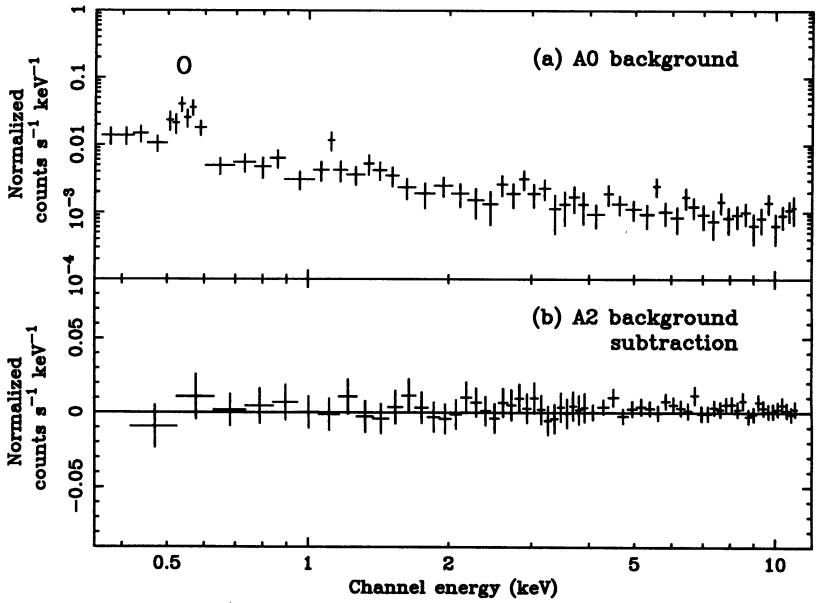

FIG. 5.—(*a*) Predicted BBXRT pixel A0 background spectrum for NGC 2110, constructed from both daytime and nighttime backgrounds. (*b*) Illustration of residuals for pixel A2 after subtracting a similarly constructed background.

night background were combined with the predicted non–X-ray background. The final background spectrum is shown in Figure 5*a*; the X-ray background here consists of about three-fourths nighttime and one-fourth daytime background. A weak oxygen line at 0.525 keV is evident in the data. The background actually dominates the total spectrum below 0.7 keV (compare with Fig. 7 below). However, the fact that BBXRT has five detector elements makes estimation of the simultaneous background fairly straightforward because the outer pixels can provide a direct estimate of the background provided that they contain no other sources. Figures 5*b* shows the residuals in pixel A2, which contains no significant source flux (see Fig. 1), after subtracting the predicted A2 background generated as described above. The reliability of the background prediction is indicated by the lack of any systematic residuals. Details of the background subtraction algorithm discussed here can be found in Weaver et al. (1995).

The NGC 2110 data from the two central pixels were modeled using the XSPEC spectral fitting package (Shafer, Haberl, & Arnaud 1989). Each BBXRT pixel has 512 energy channels. The first 15 channels in A0 and 16 channels in B0 were ignored in the spectral fitting, as these channels fall below the discriminator threshold. Channel 512 was also ignored. The remaining channels were binned to have $\sim$15–20 counts per bin in order to allow the use of χ^2 statistics. This resulted in a total of 134 bins for both source spectra combined. For the spectral analysis the A0 and B0 PHA files were fitted simultaneously, and the relative normalizations of the model components were allowed to vary. All of the fits presented here were obtained using χ^2 statistics. However, the C statistic (Cash 1979) was used on the unbinned data to test that both techniques give consistent results.

3.2. *Results*

If the BBXRT data are modeled with a power-law continuum photoelectrically absorbed by a uniform column of neutral gas,[3] the best-fit parameters are $\Gamma = 1.41 \pm 0.15[N(E) \propto E^{-\Gamma}]$, $N_{\rm H} = (2.4 \pm 0.3) \times 10^{22}$ cm^{-2}, and an observed flux of $F_{(2-10\,{\rm keV})} = 3.0 \times 10^{-11}$ ergs cm^{-2} s^{-1}. The fit is not acceptable, however, giving $\chi^2_\nu = 1.31$ for 130 degrees of freedom, i.e., there is only a 1% probability of obtaining such a large value of χ^2_ν as the result of a random fluctuation. Positive residuals between 0.6 and 1.2 keV (i.e., a soft excess) as well as residuals near 6.4 keV, can be seen in the ratio of the data to the absorbed power-law model in both A0 and B0 (Figs. 6*a* and 6*b*).

Fe Kα emission at $\sim$6.4 keV has been detected previously in many Seyfert galaxies with instruments such as *HEAO 1* and *Ginga*, and is thought to arise through reprocessing of the X-ray continuum by fluorescence of iron (less ionized than Fe XVIII) in a cold ($T \lesssim 10^5$ K) gas. The addition of a narrow (FWHM < 150 eV) Fe Kα emission feature to the model gives $\Delta\chi^2 \simeq 12$, which is significant at $\sim$97% confidence for the addition of two free parameters according to the F-test. This results in $\chi^2_\nu = 1.23$, which is still not entirely acceptable (there is only a 5% probability of exceeding this value of χ^2_ν by chance). There is no significant reduction in χ^2 when the line width is allowed to vary. The measured line energy is 6.32 ± 0.08 keV, which is consistent with the energy of cold Fe at the systemic velocity of the galaxy. The equivalent width for a narrow line in NGC 2110 is 176^{+107}_{-81} eV, and the 90% confidence upper limit on the line width is 520 eV FWHM (or 24,400 km s^{-1}). A plot of the A0 data and the power-law plus Gaussian Fe Kα line model is shown in the top panel of Figure 7.

The addition of a soft component to the power-law model significantly improves the fit. To test the sensitivity of the data to different soft excess shapes and to allow a comparison with previously published results, the parameters of simple fits to the soft excess are given in Table 1. The models used are partial covering of the direct power-law, a thermal bremsstrahlung continuum, a scattered soft X-ray continuum (as might be expected in a torus plus reflection zone model), a Gaussian line, and a Raymond-Smith plasma. All of the simple models for the soft excess adequately describe the data, resulting in acceptable values for χ^2_ν ranging from 1.09 to 1.16. A partial covering

[3] Cross sections from Morrison & McCammon (1983).

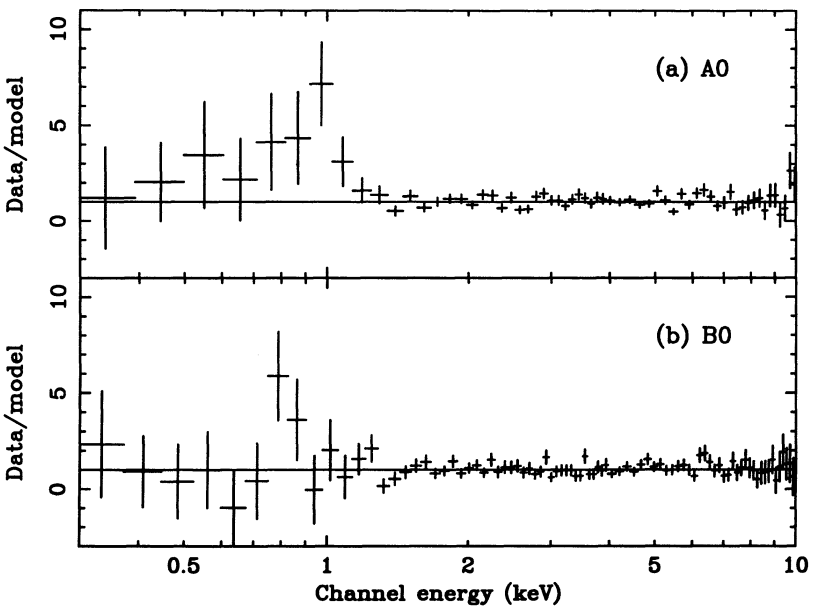

FIG. 6.—BBXRT data divided by a model consisting of a uniformly absorbed power-law. This figure illustrates the shape of the soft X-ray excess seen by BBXRT. The Fe K residuals can be seen near 6.3 keV in both the A0 and B0 spectra.

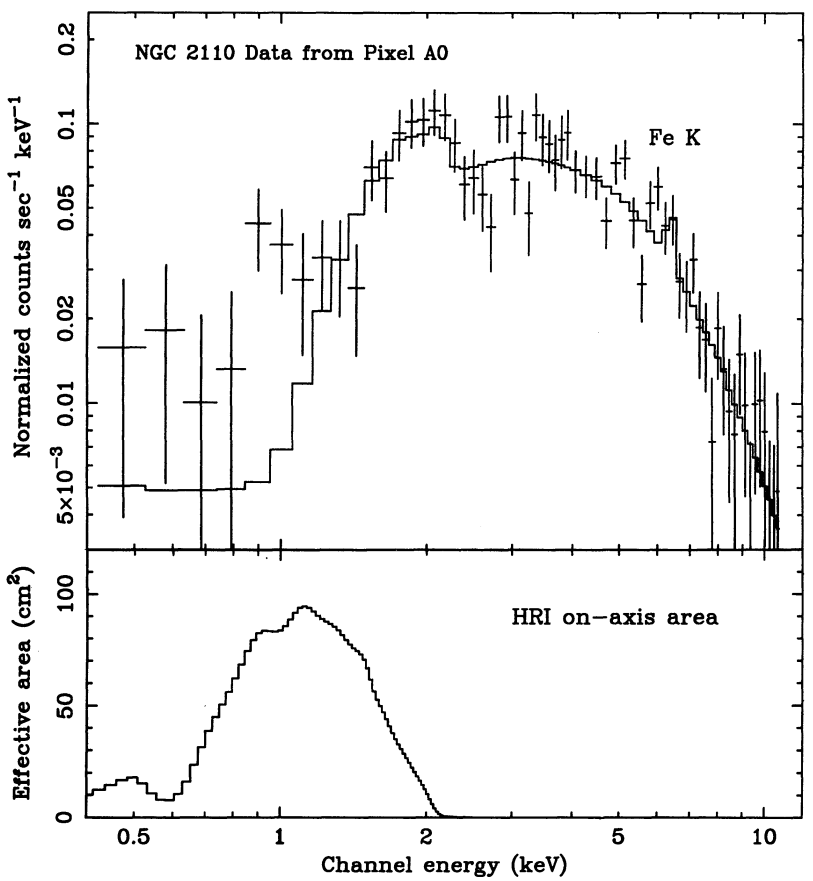

FIG. 7.—Background-subtracted BBXRT spectrum and a model (folded through the BBXRT response) that consists of a power-law continuum plus photoelectric absorption and one Gaussian emission line at 6.32 keV. The bottom panel shows the *ROSAT* HRI effective-area curve (David et al. 1992).

TABLE 1

SIMPLE MODELS FOR THE NGC 2110 SOFT EXCESS[a]

Partial Covering (Model I)	Bremsstrahlung (Model II)	Power-Law (Model III)	Gaussian Line (Model IV)	Raymond-Smith Plasma (Model V)	Notes
$\Gamma = 1.54 \pm 0.16$	$\Gamma = 1.51 \pm 0.16$	$\Gamma_1 = 1.54 \pm 0.16$	$\Gamma = 1.48 \pm 0.15$	$\Gamma = 1.50 \pm 0.05$	1
$N_H = 2.80 \pm 0.46$	$N_H = 2.77 \pm 0.49$	$N_H = 3.00 \pm 0.45$	$N_H = 2.60 \pm 0.35$	$N_H = 2.70 \pm 0.40$	2
$f_c = 0.97 \pm 0.01$	$kT \sim 0.57$ keV	$\Gamma_2 = \Gamma_1$	$E = 0.93^{+0.11}_{-0.12}$ keV	$kT = 0.88^{+0.43}_{-0.29}$ keV	
...	...	$f_{scatt} \sim 4\%$	$\sigma = 0.12^{+0.08}_{-0.06}$ keV	...	3
...	...	...	EW ~ 50 eV	...	4
$F_{soft} \sim 3.0$	$F_{soft} \sim 3.8$	$F_{soft} \sim 4.5$	$F_{soft} = (3.4 \pm 1.5)$	$F_{soft} \sim 3.0$	5
$\sim 13\%$ of total	$\sim 17\%$ of total	$\sim 19\%$ of total	$14 \pm 6\%$ of total	$\sim 13\%$ of total	6
$\chi^2/\nu = 147/126$	$\chi^2/\nu = 145/124$	$\chi^2/\nu = 146/125$	$\chi^2/\nu = 135/123$	$\chi^2/\nu = 137/124$	

NOTES.—(1) Photon index of hard X-ray continuum; (2) column density toward hard X-ray continuum; (3) line energy fixed at 0.93 keV to find the error on the width; (4) EW calculated with respect to the unabsorbed flux; (5) F_{soft} is the observed 0.1–2.4 keV flux in the soft excess given in units of 10^{-13} ergs cm^{-2} s^{-1}; (6) Percentage of the 0.1–2.4 keV flux in the soft component.

[a] N_H is given in units of 10^{22} cm^{-2}; N_H(Gal) $= 0.186 \times 10^{22}$ cm^{-2} is included in all models; a narrow Fe K feature at 6.33 keV is included in all models. The last six rows give model parameters for the soft excess.

description of the excess (model I) gives a covering fraction of 0.97 and is consistent with the *EXOSAT* result of Turner & Pounds (1989). A thermal description (model II) gives a temperature of $kT \sim 0.57$ keV, although the temperature is not well constrained. A power-law description of the soft excess (model III), representing a scattered continuum component, gives a fit of comparable quality to partial covering. In this model we find that 4% of the continuum is scattered, which is similar to the result found for a scattering description of the soft excess in NGC 4151 by Weaver et al. (1994). All three of these models give a $\Delta\chi^2$ of ~ 12, and all are statistically good descriptions of the soft excess (resulting in χ^2_ν of 1.16). However, the best fit to the soft excess ($\Delta\chi^2 = 23$ and $\chi^2_\nu = 1.09$) is obtained with a broad Gaussian centered at 0.9 keV (model IV), which would most likely represent a blend of iron L and neon K lines. The equivalent width of the Gaussian line measured with respect to the unabsorbed continuum is about 50 eV.

For a Gaussian description of the low-energy positive residuals, the soft excess makes up $\sim 14\% \pm 6\%$ of the total flux between 0.1 and 2.4 keV. At a distance of 47 Mpc, the 0.1–2.4 keV flux of $F_{soft} \sim 3.4 \times 10^{-13}$ ergs cm^{-2} s^{-1} gives a luminosity of $L_{soft} \sim 8.9 \times 10^{40}$ ergs s^{-1}. This luminosity falls well within the range of luminosities observed for the HRI extended emission ($L_{ext} = 2.3 \times 10^{40}$ to 2.6×10^{41} ergs s^{-1}), and suggests that the BBXRT soft excess is related to the soft X-ray extent. In fact, the soft excess residuals in the BBXRT data occur in precisely the ~ 1 keV region of the spectrum where the *ROSAT* HRI effective-area curve peaks (Fig. 7, *lower panel*). The HRI area curve shown in Figure 7 omits the response in the carbon band (C band) (below 0.28 keV) which contains $\sim 8\%$ of the total integrated effective area of the HRI and could, in principle, contribute signal to the HRI image. However, the large Galactic column toward NGC 2110 effectively reduces any source flux, so the response in the C band is almost zero. Because the luminosities of the extended emission and the soft excess are similar and the HRI is most sensitive at the energies where the soft excess is seen, the data strongly suggest that *the soft excess seen with BBXRT arises from the extended source seen with the HRI.*

Our result that the soft excess is not best described by a flat continuum is consistent with the majority of the soft excess shapes seen in the *Einstein* solid state spectrometer (SSS) and monitor proportional counter (MPC) data (Turner et al. 1991), which indicate that low-energy linelike features may be common in Seyfert galaxies. Turner et al. (1991) suggested that such line emission may originate from a thermal plasma that produces a blend of Fe L and Ne K emission centered around 0.8–0.9 keV. We find that a Raymond-Smith equilibrium plasma model (model V; Raymond & Smith 1977) provides a good description of the NGC 2110 soft excess, with a fit comparable to a broad Gaussian. The abundances in the model are poorly constrained by BBXRT, with a lower limit of 10% solar and an upper limit of a few times solar. The BBXRT data are also not sensitive to changes in the derived temperatures caused by altering the abundances, although this is not critical, since the emission measure of the gas only changes as $T^{1/2}$. Solar abundances have typically been assumed for the narrow-line regions of Seyfert galaxies, although both O and N appear to be overabundant by a factor of 2–3 (Storchi-Bergmann, Wilson, & Baldwin 1995). Since the BBXRT data are not sensitive to abundance differences of this size, we choose to assume solar abundances throughout. The best-fit temperature assuming solar abundances is $kT = 0.88^{+0.43}_{-0.29}$ keV, or $T = 1.02^{+0.48}_{-0.34} \times 10^7$ K. We illustrate the best-fit Raymond-Smith model for the soft excess in Figure 8. The physical implications of such a description of the excess and the extended emission are discussed further in § 4.

NGC 2110 was one of the objects suggested to have a line-like excess by Turner et al. (1991) from analysis of *Einstein* SSS data, although they report ~ 30 times more flux in the line than found here. However, the best-fit model from the SSS data is a broad line at a lower energy ($E = 0.72$ keV). Also, neither the line flux nor the column density is constrained as well with the SSS as with the BBXRT observation. The problems with modeling SSS spectra at such low energies are compounded by the fact that the usable data are cut off below 0.6 keV, just below the linelike feature. All of these differences make it difficult to make a direct comparison between the SSS and BBXRT soft excess fluxes. Therefore, we reexamined the SSS and MPC data for the observation from which a soft excess is inferred (the day 70 observation; see Turner et al. 1991). For this observation we find that the flux in the SSS soft component is 7×10^{-13} ergs cm^{-2} s^{-1} for the best-fit BBXRT Gaussian model (Table 1). This is only a factor of 2 larger than the flux seen by BBXRT. A factor of 2 difference between the fluxes at these low energies could be caused by uncertainties in the modeling of ice on the SSS detector. Therefore, the SSS data appear to be roughly consistent with the BBXRT data for a Gaussian description of the soft excess.

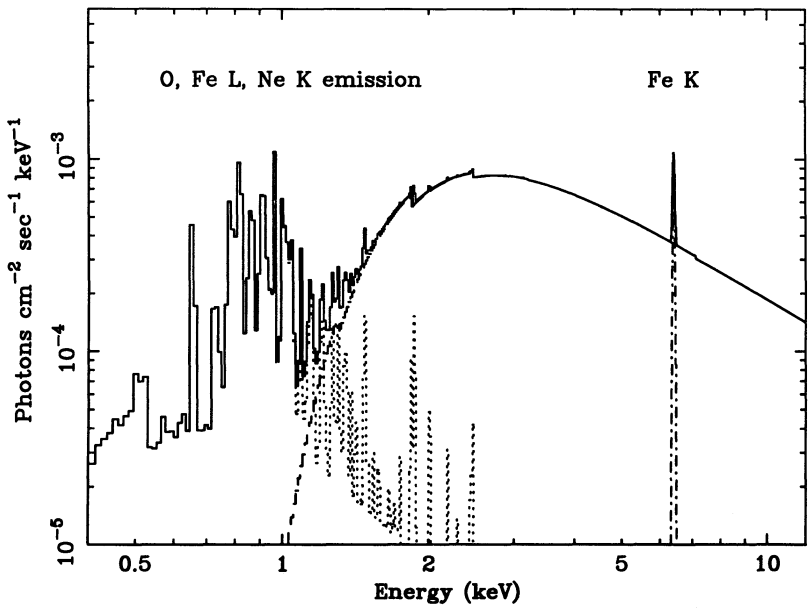

FIG. 8.—One possible model spectrum for NGC 2110, consisting of an absorbed power law, and Fe Kα line, and a Raymond-Smith plasma with $T = 1.0 \times 10^7$ K, which is dominated by line emission.

Table 2 lists the spectral parameters for NGC 2110 that have been inferred from observations since its discovery as an X-ray emitter in 1978. The 2–10 keV flux seen by BBXRT is roughly consistent with previous measurements. Over the past decade or so, the column density has remained fairly constant at $\sim 2.2 \times 10^{22}$ cm^{-2}. The only value inconsistent with this is the *HEAO 1* measurement, which has been confirmed by a recent reanalysis of the *HEAO 1* A-2 data (Weaver 1993). A significantly higher value for N_H in the *HEAO 1* data provides evidence that the column toward NGC 2110 does change. However, the absence of significant variation in the column density to NGC 2110 over the past 12 years is similar to the results for other Seyfert 2 galaxies with soft excesses, for which the columns do not vary (Mulchaey et al. 1993). Evidence that the column density does not vary on short timescales suggests, but does not prove, that the X-ray absorber is more likely to be the torus than the broad-line clouds. From this evidence, Mulchaey et al. (1993) conclude that the soft excesses in Seyfert 2 galaxies are most likely not nuclear in origin but must originate on a spatial scale larger than the torus, perhaps from the scattering zone or the narrow-line region. An extended origin for the soft excess in NGC 2110 is consistent with the lack of strong variability of the absorbing column over 12 years.

4. DISCUSSION OF SOFT X-RAY EXCESS AND EXTENT

The unique combination of the BBXRT and *ROSAT* HRI data illustrates the importance of combining spectral and spatial information in order to understand the character of soft X-ray emission in Seyfert galaxies. We find that the luminosity of the soft excess seen by BBXRT [L_{soft}(BBXRT)] is the same as the luminosity of the extended emission observed with the HRI [L_{ext}(HRI)]. This indicates that the soft excess in NGC 2110 is probably *not* nuclear in origin, but may originate from a region located $\sim 4''$ to the north of the nucleus. The coincidence of luminosities also implies that there is little extended emission on larger scales. Since the nonnuclear component is spatially unresolved in the HRI, we will assume an upper limit to its size of 8″ in diameter. For the purpose of this discussion, the distance of the X-ray source from the nucleus is $R = 920$ pc, and the radius of the extended region is $r \leq 920$ pc (§ 2).

Evidence is accumulating that spatially extended X-ray emission is common in Seyfert galaxies. Such a component has

TABLE 2

HISTORY OF SPECTRAL PARAMETERS FOR NGC 2110

EXPERIMENT	RANGE (keV)	DATE Year	DATE Day	Γ	N_H (10^{22} cm^{-2})	2–10 keV FLUX (ergs cm^{-2} s^{-1})	REFERENCE
HEAO 1 A-2.....	2.0–40.0	1978	282	1.81 ± 0.11	6.7 ± 1.1	5.0×10^{-11}	1
SSS + MPC[a].....	0.6–20.0	1979	70	$1.24^{+0.97}_{-0.71}$	$2.95^{+1.0}_{-2.9}$	3.96×10^{-11}	2
EXOSAT[a].....	0.3–20.0	1983	251	$1.64^{+0.32}_{-0.32}$	$2.23^{+1.2}_{-0.8}$	4.30×10^{-11}	3
Ginga	2.0–18.0	1989	269	$1.65^{+0.04}_{-0.03}$	$2.3^{+0.2}_{-0.2}$	3.35×10^{-11}	4
BBXRT[a].....	0.4–11.0	1990	340	1.41 ± 0.2	2.4 ± 0.5	3.0×10^{-11}	5

[a] A soft excess is either inferred or observed.

REFERENCES.—(1) Weaver 1993; (2) Turner et al. 1991; (3) Turner & Pounds 1989; (4) Nandra & Pounds 1994; (5) present analysis.

TABLE 3

SEYFERT GALAXIES SHOWING EXTENDED SOFT X-RAY EMISSION

Object	Seyfert Type	Extent (arcsec)	Radius (kpc)	Percent of Total Flux	Flux (ergs cm^{-2} s^{-1})	Luminosity (ergs s^{-1})	Reference
NGC 1068[a]	2	~30	2.2	~23	1.3×10^{-11}	$\sim 3 \times 10^{41}$	1
NGC 1566[b]	1	7.5	1.1	34	5.4×10^{-12}	$\sim 6 \times 10^{41}$	2
NGC 2110	2	~8	~1	11	$0.1\text{–}1 \times 10^{-12}$	$0.2\text{–}3 \times 10^{41}$	3
NGC 2992[b]	2	10	2.2	15	2.7×10^{-12}	$\sim 7 \times 10^{41}$	2
NGC 4151[b]	1.5	7.5	0.7	15	1.7×10^{-12}	$\sim 1 \times 10^{41}$	2
NGC 4151	1.5	20	~2.0	31	2.5×10^{-12}	$\sim 3 \times 10^{41}$	4

[a] Values listed for NGC 1068 are for the extended nuclear emission only. Emission from the starburst is not included.
[b] Flux in extended component is calculated assuming an optically thin bremsstrahlung spectrum with $kT = 3.0$ keV.
REFERENCES.—(1) Wilson et al. 1992; (2) Elvis et al. 1990; (3) this paper; (4) Morse et al. 1995.

now been detected in four other Seyfert galaxies (Table 3). The soft X-rays typically extend ~1–2 kpc and contain about 10%–30% of the total soft flux. Luminosities for the observed extended emission range from $\sim 1 \times 10^{41}$ to $\sim 1 \times 10^{42}$ ergs s^{-1}. Four out of the five objects that show extended X-ray emission are Seyfert 2 or Seyfert 1.5 galaxies. This indicates that our ability to detect soft X-ray extent may depend on the central source being suppressed at low energies, so that the extended emission is not dominated by the wings of the point-spread function from the bright nuclear continuum source. A similar argument can be applied to spectral soft excesses. In Seyfert 2 galaxies with large intrinsic absorbing columns, it is likely that we will detect weak emission in the form of soft excesses, which are swamped in most Seyfert 1 galaxies with negligible intrinsic absorption at low energies. Although several models have been proposed to explain the origin of extended X-rays in Seyfert galaxies, no firm conclusions have yet been reached.

4.1. *Partial Covering*

A simple partial covering model does not provide the most likely description of the soft excess observed in NGC 2110 (Table 1). However, such a model canot be excluded without information on spectral variability: the soft and hard components should vary together in a partial covering model. The coincidence between the fluxes in the soft excess and the extended component strongly suggests they are one and the same component. Therefore, we choose to interpret the soft excess in the BBXRT spectrum as being spatially extended in origin.

4.2. *Discrete X-Ray Sources*

It is possible that a large number of discrete X-ray sources in the galaxy may combine to produce an apparent X-ray extent. However, to account for the soft X-ray luminosity in NGC 2110 ($L \sim 9 \times 10^{40}$ ergs s^{-1}) would require 100–1000 X-ray binaries at 10^{38}–10^{39} ergs s^{-1}. This is entirely implausible because there is no evidence from other wave bands to support a large star formation rate. Long-slit spectra of NGC 2110 show purely old stellar populations, and there is no emission-line gas from H II regions (Wilson et al. 1985). Also, the optical line ratios of the narrow-line region (NLR) show the gas to be photoionized by a nonstellar continuum source (Wilson et al. 1985).

4.3. *Shock Heating*

Outflowing clouds driven by the radio jet in NGC 2110 may impact on the interstellar medium (ISM) and heat it through shocks. Such shocks could, in principle, be responsible for ionizing the gas seen in the optical emission lines and heating gas to X-ray temperatures. However, local shock heating is unlikely to produce sufficiently hot gas to account for the extended X-rays. At the location of the X-ray emission, [O III] λ5007 has a FWHM of 100–200 km s^{-1} (Wilson et al. 1985). For outflowing narrow-line clouds with this velocity, the corresponding temperature would be only ~0.1 keV or $\simeq 1 \times 10^6$ K. However, the range of temperatures of the soft component observed by **BBXRT** is 6.8×10^6 to 1.5×10^7 K for a solar abundance Raymond-Smith model and $\sim 6 \times 10^6$ K for a thermal bremsstrahlung model. These temperatures are much too high to be explained by local shock heating. Closer to the nucleus, the optical line widths reach a maximum of about 500 km s^{-1}. For clouds of this velocity, higher temperatures can be produced. Therefore, if the gas is heated by cloud-cloud or cloud-ISM collisions, then the hot gas would probably have to be generated close to the nucleus and expand in the form of a wind to a larger scale. This possibility is discussed further in § 4.6.

4.4. *Electron-scattered Nuclear Radiation*

In the unified model of Seyfert galaxies, it is thought that the hard X-rays are viewed directly through the obscuring torus (Mulchaey, Mushotzky, & Weaver 1992). It has already been found that the simplest model of this type is inconsistent with observations of NGC 4151, since an optically thick torus cannot account for both the UV and the X-ray absorption (Kriss et al. 1992, 1994; Weaver et al. 1994). However, independent of whether soft X-rays are attenuated by the torus, the broad-line region, or the accretion disk, any soft X-rays that are observed in a source with a high intrinsic column of cold gas must arise from either (1) leakage through a clumpy or ionized absorber or (2) a spatially extended region. It is certainly possible that soft X-rays can originate from the electron-scattering zone supposed to exist along the axis of the torus. In this case, the X-rays may be scattered nuclear photons, or they may originate within the scattering zone itself. Depending upon the temperature and ionization state of the scattering medium, we would expect to observe absorption and/or emission features imprinted upon the emergent X-ray spectrum. Fe L emission has already been observed in at least one other Seyfert 2 galaxy (NGC 1068), and at least part of this emission may arise in the scattering zone (Marshall et al. 1993), as was predicted by Band et al. (1990).

If we examine the simplest possible case, in which the soft excess is dominated by a scattered power-law continuum (Table 1, model III), and ignore emission from the scattering

zone itself, the fraction of the continuum that is scattered, f_{scat}, is found to be 0.04. This allows us to calculate the optical depth to Thomson scattering in the scattering zone, which is given by $\tau_{es} = f_{scat}(\Omega/4\pi)^{-1}$ for an isotropic source, where Ω is the solid angle subtended by the scattering medium at the nuclear source. If we assume an ionization cone half-opening angle of $\sim 45°$ (a solid angle of $\Omega/4\pi = 0.25$ for a one-sided cone) then $\tau_{es} = 0.16$. For an optical depth of 0.16, the radial column density of material in the scattering zone is $N_{es} = \tau_{es}/\sigma_T = 2.4 \times 10^{23}$ cm^{-2}, giving a volume density of $n \geq 42$ cm^{-3} for a radius of ≤ 0.92 kpc. For a uniform, filled cone, the mass of gas is an implausible $6 \times 10^9\ M_\odot$.

If the scattering zone were neutral, the soft X-rays would be almost entirely absorbed by such a large column of gas. So, in order for the soft X-rays to escape, the gas must be highly stripped. If this is done collisionally, temperatures greater than 3×10^6 K are needed for the scattering zone to be transparent to 0.9 keV X-rays (Krolik & Kallman 1984). However, Elvis et al. (1990) argue that for gas with such a high temperature, direct thermal emission will dominate over scattered radiation.

Alternatively, the gas may be photoionized. Assuming that this is the case, we can derive the central source luminosity needed to make the scattering zone transparent to 0.9 keV X-rays. For an optically thin gas, the ionization structure is determined by the ionization parameter, defined as

$$\xi = \frac{L_s}{nR^2}\,, \tag{1}$$

where R is the distance of the gas from the source, L_s is the luminosity of the source, and n is the electron density. If the gas is in photoionization equilibrium, then for a column of 2.4×10^{23} cm^{-2} to be transparent to 0.9 keV X-rays, the ionization parameter has to be greater than $\xi = 61$ ($\Xi = 13$; Krolik & Kallman 1984), assuming a power-law ionizing continuum with a slope of -1. To reach this level of ionization with the intrinsic nuclear source requires a central source luminosity of $L_s > 2 \times 10^{46}$ ergs s^{-1}, which is more than three orders of magnitude greater than the 0.1–2.4 keV continuum luminosity observed by BBXRT of 4×10^{42} ergs s^{-1} (corrected for absorption).

We thus conclude that, if the soft excess represents scattered nuclear X-rays, the central source must be anisotropic, radiating much more strongly toward the scattering zone than toward Earth. In a model incorporating such anisotropy, f_{scat}(anisotropic) $\sim (L_E/L_s) f_{scat}$(isotropic), where L_E and L_s are the luminosities emitted toward Earth and the scattering zone, respectively. Since f_{scat}(anisotropic) (and hence the optical depth) can be smaller than f_{scat}(isotropic), the scattering column can be smaller than in the isotropic case, and the required value of L_s lower (and more plausible) than the value calculated above. Our data cannot rule out an electron-scattering model. The anisotropy required in the model may be related to the anisotropy inferred from optical observations (Wilson et al. 1985), although the latter anisotropy may result from obscuration (Mulchaey et al. 1994).

4.5. *Line Emission*

Another possible origin for the soft excess and spatial extent is line emission, which is the best descriptor of the shape of the soft excess (§ 3.2) and can arise from photoionization. To get strong Fe L emission at ~ 0.9 keV, an ionization parameter of $\xi > 100$ is needed (Kallman & McCray 1982; Kallman 1991). Since gas is completely transparent to 0.9 keV X-rays for such a high ionization parameter (Krolik & Kallman 1984), we do not have the problem as in the electron-scattering case of the soft X-rays being absorbed by the gas.

If we assume that the region producing the lines is a sphere, the luminosity in the emission lines can be written as

$$L_{lines} = \frac{4\pi}{3}\, n^2 r^3 j(\xi)\,, \tag{2}$$

(Kallman 1991), where $j(\xi)$ is the emissivity of the photoionized gas [$j(\xi) = 10^{-24}$ ergs cm^3 s^{-1} for $\xi = 100$; T. Kallman 1993, private communication) and r is the radius of the emitting region. We have already determined the luminosity observed in the Fe L line complex to be $L_{lines} = 9 \times 10^{40}$ ergs s^{-1} (§ 3.2). Now, rearranging the above equation and substituting for L_{lines}, $j(\xi)$, and $r < 920$ pc, we find a density of $n \geq 1.0$ cm^{-3}. To determine the central source luminosity needed to ionize the gas to produce such Fe L emission, we can substitute the derived density and the ionization parameter in equation (1). For $R = 920$ pc, this gives $L_s \geq 8.0 \times 10^{44}$ ergs s^{-1}. Comparing this with the observed X-ray continuum luminosity of $L_{(1-10\,keV)} = 9 \times 10^{42}$ ergs s^{-1} (corrected for absorption), we find that the source luminosity required to produce the observed emission is almost two orders of magnitude greater than the observed X-ray continuum luminosity. As in the electron-scattering interpretation (§ 4.4), this result implies that the central hard X-ray source does not emit isotropically.

4.6. *Thermal Emission from a Plasma in Collisional Equilibrium*

For a Raymond-Smith plasma model of the BBXRT soft excess, we find $T = 10^7$ K and an emission measure n^2V of $\sim 6 \times 10^{63}$ cm^{-3}, which gives $n \geq 0.25$ cm^{-3} assuming a radius of 920 pc for the emitting region. The pressure of the X-ray–emitting gas is then $nkT \geq 3.4 \times 10^{-10}$ ergs cm^{-3}. The electron density in the optical NLR can be directly measured using the line ratio [S II] $\lambda 6716/\lambda 6731$. From a spectrum taken 5″ northwest of the nucleus, $n_{clouds} \sim 90$ cm^{-3} (Wilson et al. 1985). For a temperature of 2×10^4 K, typical of NLR clouds, we find $n_{clouds} kT_{clouds} \sim 2.5 \times 10^{-10}$ ergs cm^{-3}, which is comparable to the pressure of the gas emitting the X-rays.

In NGC 2110 the extended X-ray emission clearly appears to be associated with the forbidden-line gas (Fig. 4). It has been argued (e.g., Wolfe 1974; Krolik & Vrtilek 1984) that the cool optical emission line clouds condense out of a hot 10^6–10^7 K outflowing wind. When Compton heating and cooling are balanced, this results in a "two-phase" equilibrium for the NLR gas, a cool phase with $T_{clouds} \sim 10^4$ K and a hot phase or intercloud medium (ICM) with $T_{ICM} \sim 10^7$ K. Such a hot confining medium is necessary to keep the NLR clouds from dissipating. The pressure of the ICM would then be approximately equal to that of the clouds, giving $n_{clouds} kT_{clouds} = n_{ICM} kT_{ICM}$. The proximity of the extended X-rays and the optical high-excitation nebulosity, along with our result that the pressures of the X-ray–emitting gas and the optical line–emitting gas are comparable, suggests that the X-rays may arise from a hot gas in pressure equilibrium with the NLR.

Finally, we can determine whether the X-ray–emitting gas may comprise an outflowing wind. For our preferred temperature of 10^7 K, this gives a total thermal energy in the gas of $E_{tot} = VE_{mean}\, n \sim 3 \times 10^{55}$ ergs. Also, assuming that line emission is the best descriptor of the BBXRT soft excess, the luminosity in the lines gives a rate at which the gas in the wind is radiating energy of $dE/dt = 9 \times 10^{40}$ ergs s^{-1}. The radiative cooling time for the gas, assuming no new heat is being sup-

plied and ignoring adiabatic losses, is $t_{cool} = 1.1 \times 10^7$ yr. If the gas is an outflowing wind moving at a velocity of 200 km s^{-1}, it will travel about 2.1 kpc in the cooling time. This is similar to the distance from the nucleus and the upper limit on the size of the X-ray extent in NGC 2110. Therefore, a hot wind provides an adequate physical mechanism for the production of the extended X-rays.

4.7. *A Picture of the Central Regions of NGC 2110*

There is evidence from the scattering and photoionization descriptions of the spatially extended soft excess for an intrinsic anisotropy in the hard X-ray continuum in NGC 2110. Evidence for anisotropy has also been observed at other wave bands. First, the similarities between the morphologies of the radio "jet" and the [O III] distribution (Fig. 4) suggest either collimation or anisotropy of the ionizing photons, which may escape along and around the direction of the jet. Second, extrapolation of the observed upper limit on the nonstellar continuum at 3900 Å to shorter wavelengths provides three orders of magnitude too few ionizing photons to account for the observed Balmer recombination emission (Wilson et al. 1985). However, since UV and optical photons can easily be absorbed by the $\sim 10^{22}$ cm^{-2} column in NGC 2110, a deficiency of optical continuum photons along our line of sight may be simply a result of obscuration. Recent *HST* observations support this view (Mulchaey et al. 1994). On the other hand, hard X-rays can penetrate such columns and thus allow direct tests for intrinsic anisotropy.

A cartoon of our present model for the inner regions of NGC 2110 is shown in Figure 9. The combination of X-ray, optical, and radio data leads to a picture of NGC 2110 in which we are observing the obscuring torus more or less edge-on, with the nuclear, hard X-ray source suffering strong low-energy absorption and the broad-line region more or less blocked from direct view. The presence of an elongated morphology of the emission-line region, combined with optical photoionization arguments and a jet seen emerging from the core, suggest that the nucleus supplies energy in a collimated fashion. Additionally, there is evidence from both fluorescence and scattering descriptions of the soft X-ray excess that the hard X-ray source may be intrinsically beamed along the radio axis. A hot, pressure-driven wind, outflowing perpendicular to a collimating disk, can also explain the observed X-ray emission (similar to NGC 1068; Wilson et al. 1992), and this does not require that the X-ray source be anisotropic.

5. CONCLUSIONS

We find that a *ROSAT* HRI X-ray image of NGC 2110 consists of a point source and resolved X-ray emission, located $\sim 4''$ (~ 920 pc) from the nucleus. The extended emission is located near the optical high-excitation nebulosity, suggesting an association between the X-rays and the optical line-emitting gas. The BBXRT spectrum of NGC 2110 shows a clear soft excess which is best modeled in terms of a blend of Fe L emission centered around 0.9 keV, and that is best described as either Fe fluorescence of Fe recombination from a hot gas.

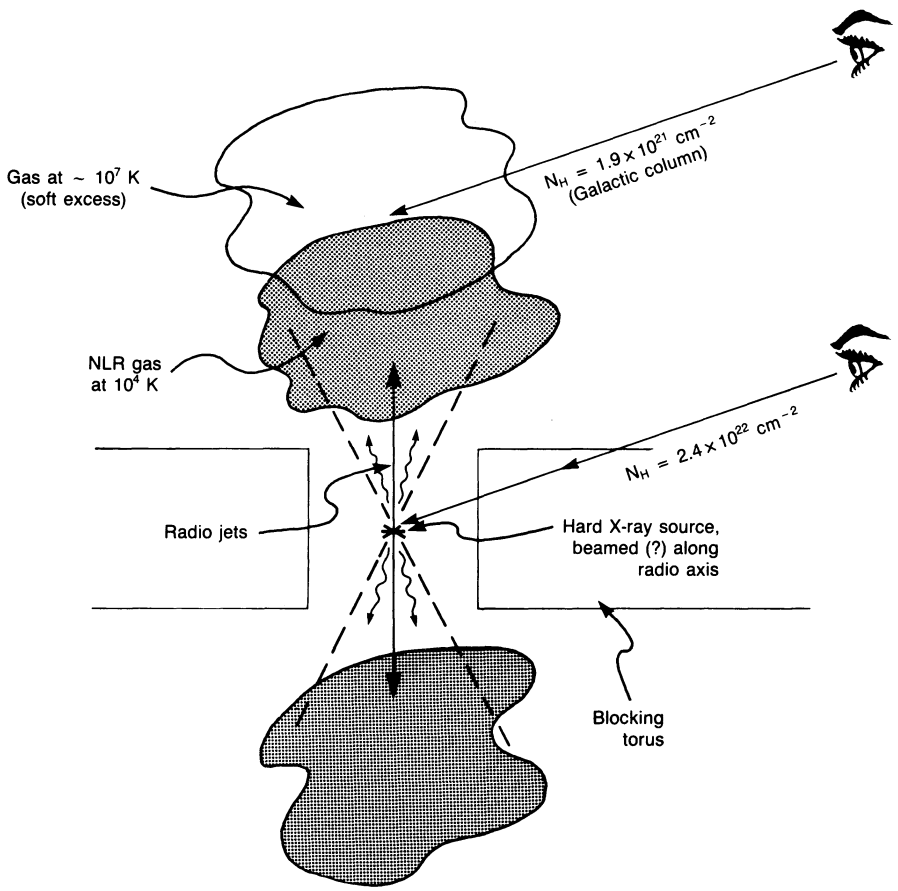

FIG. 9.—Cartoon illustrating a model for the inner regions of NGC 2110 based on radio, optical, and X-ray data.

BBXRT also confirms the presence of an Fe Kα line in NGC 2110 that has been seen previously with *Ginga*. Both the BBXRT soft excess and the HRI extended component contain $\sim$10%–15% of the total 0.1–2.4 keV flux, so L_{soft}(BBXRT) $\sim$ L_{ext}(HRI). We consider it very likely that the soft excess seen by BBXRT originates in the extended component. If this is true, the BBXRT spectrum of NGC 2110 represents the first spectrum of extended X-ray emission in a Seyfert galaxy.

If the extended soft X-ray emission in NGC 2110 results from scattering of the nuclear X-ray continuum by electrons, the required central source luminosity is over three orders of magnitude greater than the observed, absorption-corrected luminosity. Similarly, if the soft X-rays represent Fe L fluorescence, then the nuclear source luminosity required to produce the soft excess is at least two orders of magnitude higher than the unabsorbed 1–10 keV luminosity. These results suggest that the hard X-ray continuum emerges anisotropically. An alternative thermal description of the soft excess suggests that the pressure of the X-ray–emitting gas is comparable to the pressure of the narrow-line clouds. Because of the proximity of the HRI extended X-ray emission to the optical NLR, this implies that the soft excess may originate from hot gas necessary to confine at least some portion of the narrow-line clouds. If the extended emission does arise in a hot, pressure-driven wind, the X-ray continuum source is not required to be anisotropic.

This paper is the result of research toward the fulfillment of requirements of the Ph.D. degree at the University of Maryland. This research has been partially supported by a NASA Graduate Researcher's fellowship and by NASA grants NAGW-2689, NAGW-3268, and NAG8-793. M. E. also acknowledges support from NASA grant NAGW-2201. K. A. W. would like to thank Tim Kallman for insightful discussions.

REFERENCES

Band, D. L., Klein, R. I., Castor, J. I., & Nash, J. K. 1990, ApJ, 362, 90
Bradt, H. V., Burke, B. F., Canizares, C. R., Greenfield, P. E., Kelley, R. L., McClintock, J. E., van Paradijs, J., & Koski, A. T. 1978, ApJ, 226, L111
Cash, W. 1979, ApJ, 228, 939
Clements, E. D. 1983, MNRAS, 204, 811
David, L. P., Harnden, F. R., Kearns, K. E., & Zombeck, M. V. 1992, in *ROSAT* Mission Description, Appendix F, NRA 92-OSSA-16
de Vaucouleurs, G., de Vaucouleurs, A., Corwin, H. G., Buta, R. J., Paturel, G., & Fouqué, P. 1991, Third Reference Catalogue of Bright Galaxies (Austin: Univ. Texas)
Elvis, M., Fassnacht, C., Wilson, A. S., & Briel, U. 1990, ApJ, 361, 459
Elvis, M., Lockman, F. J., & Wilkes, B. J. 1989, AJ, 97, 77
Garcia, M. R., McSweeney, J. D., Karakashian, T., Thurman, J., Primini, F. A., Wilkes, B. J., & Elvis, M. 1990, The *Einstein Observatory* Database of HRI X-Ray Images Vol. 1 (CD-ROM; Smithsonian Institution Astrophysical Observatory)
Haniff, C. A., Ward, M. J., & Wilson, A. S. 1991, ApJ, 368, 167
Hasinger, G., Schmidt, M., & Trümper, J. 1991, A&A, 246, L2
Jahoda, K., et al. 1992, in The X-Ray Background, ed. X. Barcons & A. C. Fabian (Cambridge: Cambridge Univ. Press), 240
Kallman, T. R. 1991, in Iron Line Diagnostics in X-Ray Sources, ed. A. Treves, G. C. Perola, & L. Stella (Berlin: Springer), 87
Kallman, T. R., & McCray, R. 1982, ApJS, 50, 263
Kriss, G. A., et al. 1992, ApJ, 392, 485
Kriss, G., Evans, I., Ford, H., Tsvetanov, Z., Davidson, A., & Kinney, A. 1994, in The Nature of Compact Objects in AGN, ed. A. Robinson & R. J. Terlevich (Cambridge: Cambridge Univ. Press), 46
Krolik, J. H., & Kallman, T. R. 1984, ApJ, 286, 366
Krolik, J. H., & Vrtilek, J. M. 1984, ApJ, 279, 521
Marshall, F. E., et al. 1993, ApJ, 405, 168
McClintock, J. E., van Paradijs, J., Remillard, R. A., Canizares, C. R., Koski, A. T., & Véron, P. 1979, ApJ, 233, 809
Morrison, R., & McCammon, D. 1983, ApJ, 270, 119
Morse, J. A., Wilson, A. S., Elvis, M., & Weaver, K. A. 1995, ApJ, 439, 121
Mulchaey, J. S., Colbert, E., Wilson, A. S., Mushotzky, R. F., & Weaver, K. A. 1993, ApJ, 414, 144
Mulchaey, J. S., Mushotzky, R. F., & Weaver, K. A. 1992, ApJ, 390, L69
Mulchaey, J. S., Wilson, A. S., Bower, G. A., Heckman, T. M., Krolik, J. M., & Miley, G. K. 1994, ApJ, 433, 625
Mushotzky, R. F. 1982, ApJ, 256, 92
Nandra, K., & Pounds, K. A. 1994, MNRAS, 268, 405
Pogge, R. W. 1989, ApJ, 345, 730
Raymond, J. C., & Smith, B. 1977, ApJS, 35, 419
Reichert, G. A., Mushotzky, R. F., Petre, R., & Holt, S. S. 1985, ApJ, 296, 69
Serlemitsos, P. J., et al. 1992, in Frontiers of X-Ray Astronomy, ed. Y. Tanaka & K. Koyama (Tokyo: Universal Acad. Press), 221
Shafer, R. A., Haberl, F., & Arnaud, K. A. 1989, XSPEC: An X-Ray Spectral Fitting Package (ESA TM-09; Paris: ESA)
Shuder, J. M. 1980, ApJ, 240, 32
Storchi-Bergmann, Wilson, A. S., & Baldwin, J. 1995, in preparation
Tennant, A. F. 1983, Ph.D. thesis, Univ. Maryland (NASA TM 85101)
Turner, T. J., & Pounds, K. A. 1989, MNRAS, 240, 833
Turner, T. J., Weaver, K. A., Mushotzky, R. F., Holt, S. S., & Madejski, G. M. 1991, ApJ, 381, 85
Ulvestad, J. S., & Wilson, A. S. 1983, ApJ, 264, L7
Weaver, K. A. 1993, Ph.D. thesis, Univ. Maryland
Weaver, K. A., et al. 1995, ApJS, 96, 303
———. 1994, ApJ, 423, 621
Wilson, A. S., Baldwin, J. A., & Ulvestad, J. S. 1985, ApJ, 291, 627
Wilson, A. S., Elvis, M., Lawrence, A., & Bland-Hawthorn, J. 1992, ApJ, 391, L75
Wolfe, A. M. 1974, ApJ, 188, 243